EXTENDED PDF FORMAT
SPONSORED BY

BIO-RAD

http://discover.bio-rad.com



Rapid Bottom Melting Widespread near Antarctic Ice Sheet Grounding Lines

Eric Rignot, *et al.*

Science **296**, 2020 (2002);
DOI: 10.1126/science.1070942

The following resources related to this article are available online at www.sciencemag.org (this information is current as of November 27, 2006):

Updated information and services, including high-resolution figures, can be found in the online version of this article at:
http://www.sciencemag.org/cgi/content/full/296/5575/2020

This article has been **cited by** 43 article(s) on the ISI Web of Science.

This article has been **cited by** 6 articles hosted by HighWire Press; see:
http://www.sciencemag.org/cgi/content/full/296/5575/2020#otherarticles

This article appears in the following **subject collections**:
Oceanography
http://www.sciencemag.org/cgi/collection/oceans

Information about obtaining **reprints** of this article or about obtaining **permission to reproduce this article** in whole or in part can be found at:
http://www.sciencemag.org/help/about/permissions.dtl

Downloaded from www.sciencemag.org on November 27, 2006

Science (print ISSN 0036-8075; online ISSN 1095-9203) is published weekly, except the last week in December, by the American Association for the Advancement of Science, 1200 New York Avenue NW, Washington, DC 20005. Copyright c 2005 by the American Association for the Advancement of Science; all rights reserved. The title SCIENCE is a registered trademark of AAAS.

past changes in moisture availability and sources of precipitation, such as the impact on monsoon circulation caused by shifting the position of the ITCZ to a more northerly or southerly position (*14*).

References and Notes

1. G. R. Iyengar, K. J. Ramesh, R. K. Paliwal, O. P. Madan, *Curr. Sci.* **80**, 18 (2001).
2. J. R. Jones, H. Weier, P. R. Considine, *J. Oman Stud. Spec. Rep.* **3**, 61 (1988).
3. R. R. Nair *et al.*, *Nature* **338**, 749 (1989).
4. E. Van Campo, J. C. Duplessy, M. Rossignol-Strick, *Nature* **296**, 56 (1982).
5. P. D. Naidu, B. A. Malmgren, *Paleoceanography* **11**, 129 (1996).
6. S. J. Burns, A. Matter, N. Frank, A. Mangini, *Geology* **26**, 499 (1998).
7. S. J. Burns, D. Fleitmann, A. Matter, U. Neff, A. Mangini, *Geology* **29**, 623 (2001).
8. I. D. Clark, J.-C. Fontes, *Quat. Res.* **33**, 320 (1990).
9. S. C. Clemens, W. Prell, D. Murray, G. Shimmield, G. Weedon, *Nature* **353**, 720 (1991).
10. J. Overpeck, D. Anderson, S. Trumbore, W. Prell, *Clim. Dyn.* **12**, 213 (1996).
11. A.-M. Lézine, J.-F. Saliège, C. Robert, F. Wertz, M.-L. Inizan, *Quat. Res.* **50**, 290 (1998).
12. H. A. McClure, *Nature* **263**, 755 (1976).
13. F. Sirocko, M. Sarnthein, in *NATO ASI Services C* 282, M. Leinen, M. Sarnhein, Eds. (Kluwer, Dordrecht, Netherlands, 1989), pp. 401–433.
14. F. Sirocko, M. Sarnthein, H. Lange, H. Erlenkeuser, *Quat. Res.* **36**, 72 (1991).
15. S. Stokes, D. S. G. Thomas, R. Washington, *Nature* **388**, 154 (1997).
16. R. A. M. Gardner, *J. Oman Stud. Spec. Rep.* **3**, 75 (1988).
17. K. W. Glennie, in *Quaternary Deserts and Climate Change*, A. Alsharhan, K. W. Glennie, G. L. Whittle, C. G. Kendall, Eds. (Balkema, Rotterdam, Netherlands, 1998), pp. 279–291.
18. N. Juyal, A. K. Singhvi, K. W. Glennie, in *Quaternary Deserts and Climate Change*, A. Alsharhan, K. W. Glennie, G. L. Whittle, C. G. Kendall, Eds. (Balkema, Rotterdam, Netherlands, 1998), pp. 315–325.
19. Supplementary figures; details of drilling, sampling, and experimental procedures; and the luminescence data set are available on *Science* Online.
20. J. Maizels, *J. Oman Stud. Spec. Rep.* **3**, 95 (1988).
21. F. C. Bassinot *et al.*, *Earth Planet. Sci. Lett.* **126**, 91 (1994).
22. M. Rossigniol-Strick, *Nature* **304**, 46 (1983).
23. D. C. Leuschner, F. Sirocko, *Quat. Sci. Rev.* **19**, 243 (2000).
24. C. Breed *et al.*, *USGS Prof. Pap.* **1052**, 305 (1980).
25. C. E. Weyhenmeyer *et al.*, *Science* **287**, 842 (2000).
26. E. Uchupi, S. A. Swift, D. A. Ross, *Mar. Geol.* **160**, 1 (1999).
27. G. Stanger, thesis, The Open University, Milton Keynes, UK, (1986).
28. D. E. Pedgely, *Meteorol. Mag.* **99**, 29 (1970).

29. We thank W. Boenigk for allowing us to use the luminescence facilities at the Geologisches Institut, Universität zu Köln, Germany; H. U. Kasper (Geologisches Institut, Universität zu Köln) for inductively coupled plasma-mass spectrometer analyses; R. Dolhen for providing access to the γ-source at the Université Catholique de Louvain, Belgium; H. Al-Azry (Directorate of Minerals, Ministry of Commerce and Industry, Sultanate of Oman), R. Al-Abri (Al Kamil branch, Ministry of Water Resources, Sultanate of Oman), and O. Kempf (Tübingen University, Germany) for support and help during fieldwork; and C. Weyhenmeyer for constructive discussion. Financially supported by the Swiss National Science Foundation, grant no. 20-56791.99.

Supporting Online Material

www.sciencemag.org/cgi/content/full/296/5575/2018/DC1
Materials and Methods
Figs. S1 and S2
Table S1

15 January 2002; accepted 2 May 2002

Rapid Bottom Melting Widespread near Antarctic Ice Sheet Grounding Lines

Eric Rignot[1]* and Stanley S. Jacobs[2]*

As continental ice from Antarctica reaches the grounding line and begins to float, its underside melts into the ocean. Results obtained with satellite radar interferometry reveal that bottom melt rates experienced by large outlet glaciers near their grounding lines are far higher than generally assumed. The melting rate is positively correlated with thermal forcing, increasing by 1 meter per year for each 0.1°C rise in ocean temperature. Where deep water has direct access to grounding lines, glaciers and ice shelves are vulnerable to ongoing increases in ocean temperature.

The undersides of ice streams flowing from the Antarctic continent typically melt into the ocean where they cross the grounding line and begin to float as ice shelves and ice tongues (*1*). Unlike melting under the grounded ice sheet, processes beneath floating glaciers are governed by the transport of ocean heat and by the seawater freezing temperature dependence on pressure (*2*). This allows sensible heat to be obtained from the cold, dense shelf waters resulting from sea ice formation, as well as "warm" deep water that intrudes onto the continental shelf and flows into ice shelf cavities. Bottom melting freshens and cools the seawater, adding buoyancy that drives upwelling as the ice shoals seaward. In some regions, the rising seawater-meltwater mixture drops below the in situ freezing point to form "marine" ice that can comprise a substantial part of ice shelf volume (*3*, *4*). Where the continental shelf is broad and the inflows are cold and dense, some of the meltwater-laden outflows eventually sink and contribute to the formation of bottom water, which ventilates the deepest parts of the world's oceans (*5*). Net basal melting beneath the 1.6×10^6 km^2 floating portion of the Antarctic Ice Sheet (*6*), adjusted for recent lower estimates for the larger ice shelves (*4*, *7*), is believed to be around 40 cm/year. But much of the actual melting occurs in the deepest parts of the sub–ice shelf cavities, where direct measurements are unavailable and would be very difficult to acquire.

Here we calculate basal melt rates at 23 of these remote interior regions, using satellite radar interferometry observations of grounding line position, ice velocity, and surface topography of outlet glaciers that nourish the ice shelves and ice tongues (*8*). With this technique, grounding lines can be precisely located and are often found to lie tens of kilometers landward of previously estimated positions (*9*). Basal melting calculations assume mass conservation and steady-state conditions between the grounding line and a flux gate located about one glacier-width downstream (*10*). Thickness changes due to short-term changes in creep rate, snow accumulation, and surface ablation are believed to be small compared with the large bottom melt rates obtained.

We focus on melt rates near the grounding lines of deep-draft outlet glaciers because continental ice discharge is principally controlled by the channeled flow of these ice streams into the ocean (Fig. 1). If these regions are the locus of high basal melting, the potential exists for substantial ocean control over ice shelf, if not ice sheet, mass balance (*11*–*13*). Indirect observations and computer models have suggested high basal melting in the proximity of deep grounding lines and have shown that melting efficiency will decrease as buoyant plumes lose heat and rise to shallower depths along ice-ocean interfaces (*14*, *15*). Therefore, it is not the average ice shelf melt rate but the melt rate near the grounding line that will have the greatest impact on ice flow dynamics. As the properties and circulation of the ocean are modified by climate change, a corresponding change in the rate of basal melting in this region may alter ice thickness, move grounding lines, and accelerate the flow of ice into the sea.

The basal melt rates for the 23 glaciers shown in Fig. 1 are listed in Table 1. The spectrum of values ranges from <4 m/year for several glaciers that flow into the Filchner-Ronne Ice Shelves to >40 m/year for Pine Island Glacier. The wide range is consistent with earlier studies of several of the individual glaciers, using a variety of methods (*16*–*21*), and stems from quite different grounding line drafts, seawater temperatures,

[1]Jet Propulsion Laboratory, California Institute of Technology, Mail Stop 300-235, Pasadena, CA 91109–8099, USA. [2]Lamont-Doherty Earth Observatory, Columbia University, Route 9W, Palisades, NY 10964–8000, USA.

*To whom correspondence should be addressed. E-mail: eric@adelie.jpl.nasa.gov (E.R.); sjacobs@ldeo.columbia.edu (S.S.J.)

Downloaded from www.sciencemag.org on November 27, 2006

and ice topographies and velocities. Nevertheless, most of the melt rates we calculate near glacier grounding lines exceed the area-average rates for the largest ice shelves by 1 to 2 orders of magnitude.

The melt rates listed in Table 1 are strongly correlated with ocean thermal forcing (Fig. 2), with a correlation $R > 0.85$. The lateral spread of values around a linear regression results from uncertainties in ocean temperature, ice thickness, and the assumption of steady state. The use of maximum draft for the calculation slightly overestimates thermal driving, increasing R by 0.03 and decreasing the regression slope by 10%. Melt rate also depends on how rapidly ocean heat can be delivered to the basal ice, which is, in turn, a function of the density field, tidal mixing, sea floor topography, and cavity shape (*22*, *23*). Those factors vary locally and are not well known, possibly leading to divergent melt rates for glaciers with similar grounding line ice flux and ocean forcing, e.g., Mertz and Ninnis glaciers in Table 1. The floating tongues of those glaciers presently appear to be at opposite ends of advance and decay cycles (*24*) and have grounding lines at different distances from the general trend of the coastline, which could be important (*17*). The weakly melting Ninnis remnant has also been accompanied for more than a decade by large grounded icebergs that may reduce the strength of the local circulation (*25*) and its temperature.

The largest thermal forcing, nearly 4°C above the in situ melting point (Fig. 2), is associated with the Pine Island, Thwaites, and Smith glaciers that flow into the Amundsen Sea. This results from the nearly unaltered circumpolar deep water that extends southward across the floor of the Antarctic continental shelf in Pine Island Bay (*6*). The poor fit for Smith Glacier could indicate a blocking sill between its grounding line and deep water in the Bay, consistent with the presence of numerous ice rises in radar interferometry observations of the ice shelf. Deep water influence wanes toward the west but clearly impacts the Kohler, DeVicq, and Land glaciers (Table 1). Water warmer than +1.0°C also floods the deeper shelf regions in the Bellingshausen Sea, but its effects are proportional to grounding line depth. Ocean temperatures of –2°C were assumed beneath glaciers entering the large ice shelves, from measurements beneath the western Ronne Ice Shelf (*7*), except that −2.2°C temperatures were assumed beneath glaciers draining into the Filchner-Ronne Ice Shelf east of 75°W (*26*). Ocean temperatures will be colder [smaller thermal forcing (ΔT) in Table 1] if the outflow from a deep grounding line, e.g., 2.0 km for Foundation Ice Stream (*16*), is advected past a shallower grounding line downstream (Institute and Ronne at 1.2 km).

The basal melt rate/ΔT ($B/\Delta T$) ratio of ~10/1 (m/°C) in Fig. 2 is similar to relations obtained for icebergs melting in warmer ocean water and in a related laboratory experiment (*27*, *28*). However, what has not been clear is whether such high rates also applied in seawater at and below the surface freezing point on the Antarctic continental shelf. We now see that where grounding lines are deep, melt rates can exceed 10 m/year in frigid seawater that results from sea ice formation. Indeed, the melting points for the peak ice thickness at the grounding line (H_p) drafts in this study range from –2.6 to –4.0°C. Thermal forcing is thus high for

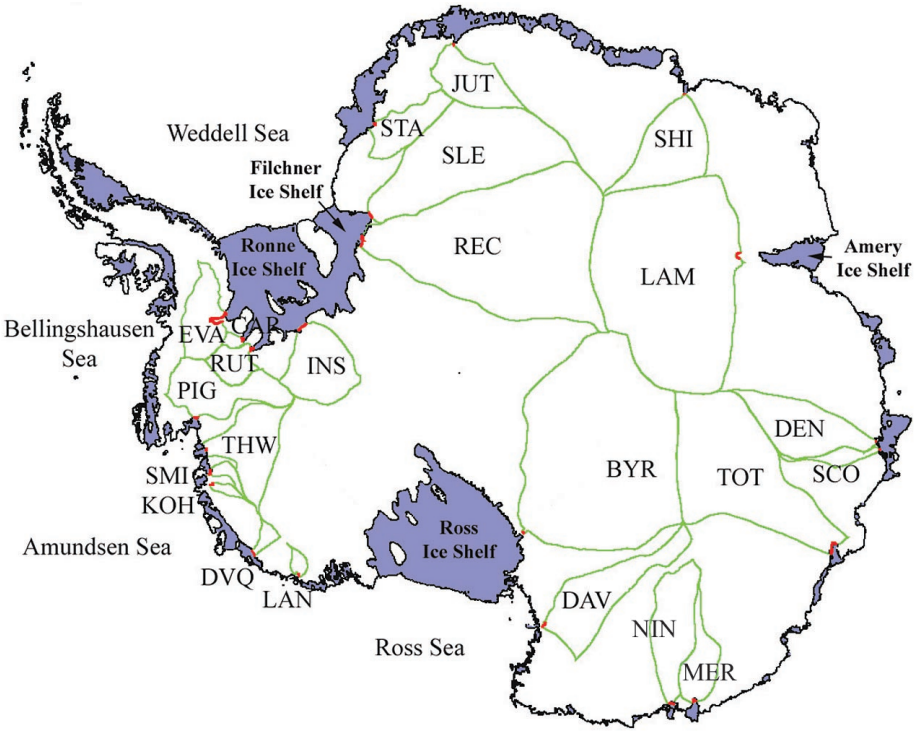


Fig. 1. Location map of the 23 Antarctic glaciers and ice shelves listed in Table 1. The Antarctic Data Base coastlines (*9*) (ice front position and grounding line) are black, the drainage basins are outlined in green, the Interferometric Synthetic Aperture Radar (InSAR)-derived grounding line flux gates are red, and ice shelves and floating tongues are blue. The 23 glaciers together drain more than 1/3 of the area of continental Antarctica, funneling the ice via a network of ice streams through narrow exit gates. Abbreviations for glaciers and ice shelf extensions are as follows: Pine Island (PIG), Thwaites (THW), Smith and Crosson (SMI), Kohler and Dotson (KOH), DeVicq and Getz (DVQ), Land (LAN), Byrd and Ross (BYR), David and Drygalski (DAV), Ninnis (NIN), Mertz (MER), Totten (TOT), Denman and Shackleton (DEN), Scott and Shackleton (SCO), Lambert and Amery (LAM), Shirase (SHI), Jutulstraumen and Fimbul (JUT), Stancomb-Wills (STA), Slessor and Filchner (SLE), Recovery and Filchner (REC), Institute and Ronne (INS), Rutford and Ronne (RUT), Carlson and Ronne (CAR), and Evans and Ronne (EVA).

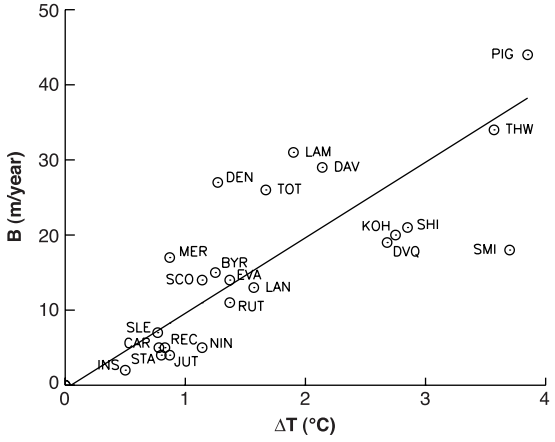


Fig. 2. Basal melt rates directly seaward of the grounding lines of Antarctic glaciers versus thermal forcing by the ocean. B is calculated from satellite radar interferometry observations of ice velocity and applies to the ice shelf area between the grounding line and a flux gate located about one glacier-width downstream. ΔT is the difference between the nearest in situ ocean temperature measurement and the seawater freezing point (*43*) at a depth of 0.88 H_p [Table 1, (*21*)]. The regression, $B = 10.06\Delta T - 0.48$, R = 0.92, and without Smith Glacier (SMI) but with a single control at (0, 0), indicates that a 1°C increase in effective ocean temperature will increase the melt rate by 10 m/year. Power relations of the type predicted for tidally induced basal melting (*22*) or a laboratory experiment using warmer water (*28*) fit these data less well, but would alter for rates of change at the thermal forcing extrema.

Downloaded from www.sciencemag.org on November 27, 2006

glaciers like Lambert and David, which have grounding lines that reach depths of 3 km below sea level (Table 1). As a result, David Glacier loses 68% of its mass from bottom melting within 20 km of the grounding line, driving an upwelling of "supercooled" water and the possible deposition of enough marine ice to preserve a lengthy Drygalski Ice Tongue (*17*).

The Shirase Glacier in East Antarctica has a relatively shallow grounding line (Table 1) in a region generally characterized by cold shelf water. Its high thermal forcing results from April and August ocean temperatures of +0.15°C at depths below 900 m, landward of a sill on the outer shelf (*29*). This indicates that relatively warm "modified" deep water has year-round access to the Shirase grounding line. Modified circumpolar deep water is known to upwell at other locations along the East Antarctic continental shelf and will increase grounding line melt rates where its density allows it to intrude along the sea floor.

Our results demonstrate that bottom melting near an ice shelf grounding line is strongly leveraged by the temperature of seawater that comes into contact with the ice in that region. A rise in ocean temperature that increases the bottom melt rate will steepen the ice thickness gradient near the grounding line. That will increase the driving stress and flow velocity, and it will reduce the ice shelf resistance to ice discharge, potentially causing the glacier to accelerate and its grounding line to retreat. If enhanced melting caused a grounding line to move landward into a deeper basin, a positive feedback will occur as the ocean progressively reaches deeper ice. Conversely, a decrease in the melt rate, or a grounding line moving upslope, would stabilize the glacier by thickening and lowering its velocity (*13*).

Although the dynamic coupling between grounded and floating ice is complex, ice flow models have been developed to predict the response of the Antarctic Ice Sheet to a change in climate (*30*, *31*). Such models show that ice sheet area and volume would decline if area-averaged ice shelf melt rates increased 1 m/year above steady-state conditions but do not address the issue of much higher and changing melt rates focused near the grounding lines. It has been noted (*32*) that warmer winters and reduced sea ice production would likely alter the flow of dense shelf water beneath the ice, decreasing bottom melting if that inflow were not replaced by warm deep water. The projected melt reduction in that scenario is only 10%, however, for an air temperature rise of 3°C in a century. Air temperature has risen at that rate over recent decades at Scott Base in the southwest Ross Sea, where shelf water salinity has declined over the same period (*33*). The salinity change appears to have resulted from freshwater sources upstream of the Ross Sea continental shelf, including the melting of continental ice.

Table 1. Basal melt rates of Antarctic glaciers directly seaward of their grounding lines, assuming steady-state conditions. Year, year in which ice velocity was measured (1992, 1994, and 1996 are ERS-1/2; 1997 is Radarsat-1); shown in parentheses after H_p are mean values. Meters/year and km^3/year are in ice equivalent (see Fig. 2) (*10*). The flux gates of THW, SMI, LAN, STA, and REC only encompass the central, faster-moving, thicker part of those glaciers (Fig. 1).

Glacier	Year	H_p (km)	Φ_{GL} (km^3/year)	*ISA* (km^2)	Φ_{DG} (km^3/year)	*B* (m/year)	ΔT (°C)
PIG	1996	1.3 (1.0)	75.1 ± 4	795	40.1 ± 2	44 ± 6	3.9
THW	1996	1.0 (0.9)	36.0 ± 3	413	21.8 ± 2	34 ± 9	3.6
SMI	1996	1.2 (1.0)	19.3 ± 2	341	13.1 ± 1	18 ± 8	3.7
KOH	1996	1.2 (1.1)	9.9 ± 1	210	5.8 ± 0.5	20 ± 5	2.8
DVQ	1996	1.1 (0.8)	18.7 ± 2	384	11.4 ± 1	19 ± 6	2.7
LAN	1996	1.0 (0.9)	11.1 ± 1	167	8.9 ± 1	13 ± 6	1.6
BYR	1997	1.9 (1.8)	23.5 ± 2	544	15.1 ± 1	15 ± 4	1.3
DAV	1996	3.2 (1.9)	15.6 ± 2	362	5.0 ± 0.5	29 ± 5	2.1
NIN	1996	1.7 (1.2)	21.9 ± 3	406	19.9 ± 2	5 ± 7	1.1
MER	1996	1.3 (1.1)	19.1 ± 2	375	12.9 ± 1	17 ± 6	0.9
TOT	1996	2.5 (1.7)	69.6 ± 7	1030	42.9 ± 4	26 ± 8	1.7
DEN	1996	1.9 (1.8)	31.9 ± 4	616	15.3 ± 2	27 ± 7	1.3
SCO	1996	1.7 (1.3)	9.2 ± 2	482	2.3 ± 0.5	14 ± 4	1.1
LAM	1996	3.0 (2.3)	57.5 ± 5	952	28.4 ± 2	31 ± 5	1.9
SHI	1996	1.2 (0.9)	15.1 ± 2	214	10.6 ± 1	21 ± 10	2.9
JUT	1994	1.3 (1.2)	13.4 ± 1	391	11.9 ± 1	4 ± 3	0.9
STA	1996	1.2 (0.9)	16.6 ± 2	465	14.8 ± 1	4 ± 4	0.8
SLE	1997	1.6 (1.4)	31.6 ± 2	940	25.2 ± 2	7 ± 2	0.8
REC	1997	1.7 (1.3)	30.7 ± 3	748	26.7 ± 2	5 ± 5	0.7
INS	1997	1.2 (1.1)	26.0 ± 2	1101	23.4 ± 2	2 ± 3	0.5
RUT	1992	2.2 (1.7)	17.6 ± 2	785	8.7 ± 1	11 ± 3	1.4
CAR	1992	1.4 (1.4)	2.6 ± 0.2	362	1.0 ± 0.1	5 ± 1	0.8
EVA	1996	2.2 (1.5)	50.6 ± 5	2205	18.9 ± 2	14 ± 2	1.4

The potential impact of basal melting on short-term (less than a century) ice sheet stability is greatest in regions where deep water has direct access to glacier grounding lines. Those areas now occur mainly in the South-East Pacific–West Antarctic sector (*6*) but also include East Antarctica, as shown by the Shirase Glacier. It remains to be determined how much a stronger pycnocline beneath a fresher surface layer will increase the temperature of warm deep water (*34*), and whether less sea ice and dense shelf water production or increased melting of glacier ice will change the transport of that deep water onto the Antarctic continental shelf. Ocean temperatures directly seaward of Antarctica's continental shelf break have risen by ~0.2°C over recent decades (*33*, *35*), which is sufficient to increase basal melting by ~2 m/year where that change has reached vulnerable grounding lines. This may account for the rapid thinning of ice shelves in the western Amundsen Sea (*20*, *21*, *36*, *37*), which, in turn, may play an essential role in the observed acceleration of their nourishing glaciers (*38*).

References and Notes

1. G. de Q. Robin, *J. Glaciol.* **24**, 259 (1979).
2. C. S. M. Doake, *Polar Rec.* **18**, 37 (1976).
3. H. Oerter *et al.*, *Nature* **358**, 399 (1992).
4. K. Grosfeld *et al.*, *Antarct. Res. Ser.* **75**, 83 (1998).
5. A. H. Orsi, S. S. Jacobs, A. L. Gordon, M. Visbeck, *Geophys. Res. Lett.* **28**, 2923 (2001).
6. S. S. Jacobs, H. H. Hellmer, A. Jenkins, *Geophys. Res. Lett.* **23**, 957 (1996).
7. K. W. Nicholls, K. Makinson, *Antarct. Res. Ser.* **75**, 301 (1998).
8. Grounding lines were mapped using a differential interferometry technique applied to European Remote Sensor (ERS) radar data collected in 1992, 1994, and 1996 with a positional accuracy of 50 m (*39*) (Table 1). Ice velocity was mapped in vector form with ERS interferometry data collected north of 79°S latitude with a precision of a few meters per year where crossing swaths were available, otherwise combining interferometry data with speckle tracking along the satellite track with a precision of a few tens of meters per year (*40*). Velocity control was provided by motionless areas. Tidal corrections were applied on observed ice shelf velocities using predictions from the FES99 tidal model (*41*). For glaciers located south of 79°S latitude, we employed Radarsat radar data collected in 1997 to map the ice velocity using speckle tracking both along and across the satellite track directions, with a precision of a few meters per year. The grounding line position of the glaciers surveyed in 1997 with Radarsat was inferred from hydrostatic equilibrium of the ice (no differential interferometry data were collected during that survey), with a precision of 1 km, by comparing ice shelf elevations with BEDMAP thicknesses (*42*). Grounding line ice thickness for all glaciers was inferred from hydrostatic equilibrium constrained by existing thickness measurements where available, and assuming a default seawater and ice density profile elsewhere.
9. British Antarctic Survey's Antarctic Digital Data Base is available online at: www.nerc-bas.ac.uk/public/magic/add_main.html.
10. Conservation of ice mass between the grounding line (GL) and a flux gate located downstream (DG), bordered by distinct flow bands, dictates that ice shelf thickening over the ice shelf area, *ISA*, between the two gates, $\partial H/\partial t$ (positive for thickening), equals the sum of surface accumulation, *A*, minus the basal

Downloaded from www.sciencemag.org on November 27, 2006

accumulation, B (positive for melting), and the difference in ice flux between the two gates per unit area, $\partial H / \partial t = A - B + (\phi_{GL} - \phi_{DG})/ISA$, where ϕ_{GL} and ϕ_{DG} are the ice flux for the GL and the DG, respectively. Under steady-state conditions, $\partial H / \partial t = 0$, and neglecting surface melt and accumulation (<0.5 m/year) compared with basal melting, B is equal to the decrease in ice flux per unit area. If the ice shelf is thickening (thinning) and ice flow is steady, then B would be lower (higher) than calculated under steady-state conditions.

11. J. Weertman, *J. Glaciol.* **13**, 3 (1974).
12. C. J. Van der Veen, *Ann. Geophys. Ser. B* **4**, 45 (1986).
13. R. H. Thomas, *J. Glaciol.* **24**, 167 (1989).
14. H. H. Hellmer, S. S. Jacobs, A. Jenkins, *Antarct. Res. Ser.* **75**, 83 (1998).
15. A. Jenkins, in *Ice in the Climate System*, W. R. Peltier, Ed. (Springer-Verlag, Berlin, 1993), pp. 217–235.
16. A. Lambrecht, C. Mayer, H. Oerter, U. Nixdorf, *Ann. Glaciol.* **29**, 250 (1999).
17. M. Frezzotti, I. E. Tabacco, A. Zirizzotti, *Ann. Glaciol.* **46**, 253 (2000).
18. A. M. Smith, *J. Geophys. Res.* **101**, 22749 (1996).
19. J. R. Potter, J. G. Paren, *Antarct. Res. Ser.* **43**, 35 (1985).
20. E. Rignot, *Science* **281**, 549 (1998).
21. _____, *J. Glaciol.* **47**, 213 (2001).
22. D. R. MacAyeal, *J. Geophys. Res.* **89**, 597 (1984).
23. K. Makinson, *J. Phys. Oceanogr.* **32**, 202 (2002).
24. G. Wendler, K. Ahlnas, C. S. Lingle, *J. Glaciol.* **42**, 447 (1996).
25. O. A. Nøst, S. Østerhus, *Antarct. Res. Ser.* **75**, 267 (1998).
26. K. W. Nicholls, S. Østerhus, K. Makinson, M. R. Johnson, *J. Geophys. Res.* **106**, 11481 (2001).
27. W. F. Budd, B. J. McInnes, D. Jenssen, I. N. Smith, in *Dynamics of the West Antarctic Ice Sheet*, C. J. van der Veen, J. Oerlemans, Eds. (Kluwer Academic, Dordrecht, Netherlands, 1987), pp. 322–360.
28. D. S. Russell-Head, *Ann. Glaciol.* **1**, 119 (1980).
29. S. Ushio, T. Takizawa, "Oceanographic data in Lutzow-Holm Bay of Antarctic Climate Research Programme from March 1990 to January 1991," vol. 184 of Japanese Antarctic Research Expedition Data Reports (National Institute of Polar Research, Tokyo, 1993).
30. P. Huybrechts, J. de Wolde, *J. Clim.* **12**, 2169 (1999).
31. R. C. Warner, W. F. Budd, *Ann. Glaciol.* **27**, 161 (1998).
32. K. Nicholls, *Nature* **388**, 460 (1997).
33. S. S. Jacobs, C. F. Giuvili, P. A. Mele, *Science*, in press.
34. A. Gordon, Proceedings of the *CO_2 Research Conference on Science and Consensus*, 19 to 23 September 1982, Berkeley Springs, VA (Institute for Energy Analysis, Washington, DC, 1983), pp. IV.76–IV.86.
35. R. Robertson, M. Visbek, A. L. Gordon, E. Fahrbach, *Deep-Sea Res.*, in press.
36. J. Zwally, personal communication.
37. A. Shepherd, D. J. Wingham, J. A. D. Mansley, H. F. J. Corr, *Science* **291**, 862 (2001).
38. E. Rignot, D. G. Vaughan, M. Schmeltz, T. Dupont, D. MacAyeal, *Ann. Glaciol.* **34**, 189 (2002).
39. E. Rignot, S. Gogineni, W. Krabill, S. Ekholm, *Science* **276**, 934 (1997).
40. R. Michel, E. Rignot, *J. Glaciol.* **45**, 93 (1999).
41. F. Lefevre, F. H. Lyard, C. Le Provost, *Geophys. Res. Lett.* **27**, 2717 (2000).
42. M. B. Lythe, D. G. Vaughan, *J. Geophys. Res.* **106**, 11335 (2001).
43. "Freezing point of seawater," in the *Eighth Report of the Joint Panel of Oceanographic Tables and Standards*, *UNESCO Tech. Pap. Mar. Sci. 28* (1978), pp. 29–35.
44. We thank the European Space Agency, the Canadian Space Agency, and the Alaska SAR Facility for providing the ERS and Radarsat satellite data used in this project. Manuscript reviews helped to focus the discussion. Funding for this project was provided by a research contract with the National Aeronautics and Space Administration's Cryospheric Sciences Program and by the National Science Foundation, Office of Polar Programs.

15 February 2002; accepted 16 April 2002

Hybridization and the Evolution of Reef Coral Diversity

Steven V. Vollmer* and Stephen R. Palumbi

Hundreds of coral species coexist sympatrically on reefs, reproducing in mass-spawning events where hybridization appears common. In the Caribbean, DNA sequence data from all three sympatric *Acropora* corals show that mass spawning does not erode species barriers. Species *A. cervicornis* and *A. palmata* are distinct at two nuclear loci or share ancestral alleles. Morphotypes historically given the name *Acropora prolifera* are entirely F_1 hybrids of these two species, showing morphologies that depend on which species provides the egg for hybridization. Although selection limits the evolutionary potential of hybrids, F_1 individuals can reproduce asexually and form long-lived, potentially immortal hybrids with unique morphologies.

Diverse reef-building coral assemblages have served as the foundation for complex reef ecosystems with exceptional biodiversity and productivity. Yet, the evolutionary genesis of coral diversity remains mired in a paradox. As many as 105 coral species from 36 genera and 11 families reproduce in yearly, synchronous mass-spawning events (*1*), thereby providing overwhelming opportunities for hybridization among congenerics (*2*). Laboratory crosses from a number of mass-spawning genera demonstrate that viable hybrids occur among congenerics (*2*, *3*). Interspecific hybridization should blur coral species boundaries and stifle species diversification, yet many mass-spawning coral groups have rapidly diversified. The juxtaposition of high hybridization potential and high species diversity in mass-spawning corals has confused the picture of coral evolution and cast such doubt on the cohesiveness of coral species boundaries (*4*) that some species-rich genera have been considered hybrid swarms (*3*). *Acropora*, the world's most speciose coral group (*5*), exemplify this view (*2*–*4*). Most of the 115 species of *Acropora* arose over the past 5 million years (My) (*6*, *7*), and many are capable of hybridizing with sympatric congenerics in laboratory crosses (*2*, *8*). One prominent hypothesis proposes that interspecific hybridization promotes reticulate evolution and morphological diversification in the absence of genetically distinct species (*3*), even though a genetic mechanism for this

Department of Organismic and Evolutionary Biology, Harvard University, 16 Divinity Avenue, Cambridge, MA 02138, USA.

*To whom correspondence should be addressed. E-mail: svollmer@oeb.harvard.edu

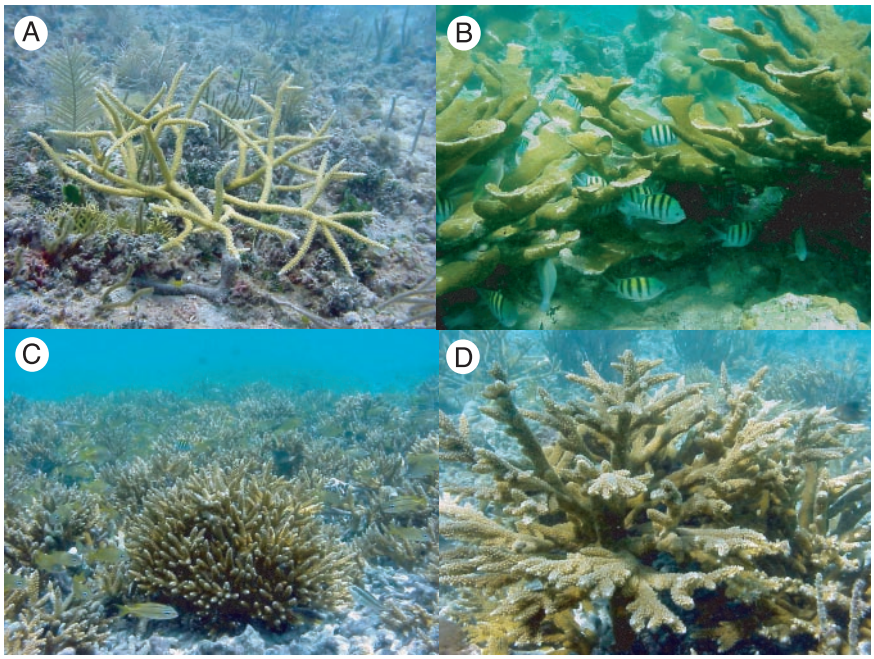


Fig. 1. The Caribbean *Acropora* species: (**A**) *A. cervicornis* and (**B**) *A. palmata*, and (**C**) the bushy and (**D**) palmate F_1 hybrid *A. prolifera* morphs from Puerto Rico.

Downloaded from www.sciencemag.org on November 27, 2006